Article

Simple Metal and Binary Alloy Phases Based on the *fcc* Structure: Electronic Origin of Distortions, Superlattices and Vacancies

Valentina F. Degtyareva and Nataliya S. Afonikova

Institute of Solid State Physics, Russian Academy of Sciences, Chernogolovka 142432, Russia;
E-mail: degtyar@issp.ac.ru

Abstract: Crystal structures of simple metals and binary alloy phases based on the face-centered cubic (*fcc*) structure are analyzed within the model of Fermi sphere – Brillouin zone interactions to understand the stability of original cubic structure and derivative structures with distortions, superlattices and vacancies. Examination of the Brillouin-Jones configuration in relation to the nearly-free electron Fermi sphere for several representative phases reveals significance of the electron energy contribution to the phase stability. Representation of complex structures in the reciprocal space clarifies their relationship to the basic cubic cell.

Keywords: crystal structure; Hume-Rothery phases; structure stability

1. Introduction

Crystal structures of metals have three principal lattices: face-centered cubic (*fcc*), close-packed hexagonal (*hcp*) and body-centered cubic (*bcc*) with high symmetry and a close packing atomic arrangement. The prevalence of these structures is determined by high symmetry and high coordination numbers with the resulting high values of the Madelung constant and low electrostatic term of the crystal energy, called Ewald energy, E_{Ewald}. Another significant crystal energy term is the band structure energy, E_{BS}, defined by ion-electron interactions for a given structure.

Intermetallic compounds are mostly based on these types of structures with deformations, superlattices and vacancies, caused by differences in atomic sizes and electronegativities of components. One of key factors for phase stability is "electron concentration" – a number of valence electrons per atom [1-3]. Crystal energy is reduced due to the level of the valence electron energy (Fermi level) approaching the Brillouin zone plane and causing a formation of the energy gap.

The binary alloy system Cu – Zn represents a classical example of Hume-Rothery phases that include the key metallic close-packed structures: *fcc*, *hcp* and *bcc*. The sequence of the phases as a function of the average number of valence electrons per atom *fcc* → *bcc* → complex γ-phase → *hcp* is defined by the following values of the valence electron concentration 1.35 →1.5 → 1.62 → 1.75 (electron/atom). Similar phase sequences have been observed in many other binary alloy systems containing a noble metal from the group I B and a neighboring element from groups II B – V B. The Cu – Zn alloy system is a relatively simple system with only five intermediate phases that exhibit quite simple structures with the ground high-symmetry metallic phases like *fcc*, *bcc* and *hcp*. Along with these basic metallic structures there are phases Cu_5Zn_8-*cI*52 and $CuZn_3$-*hP*3 that are related to *bcc* through superlattices, distortions and vacancies. In our previous papers we have considered metallic phases based on the *bcc* and *hcp* structures [4, 5]. Recently we have considered intermediate phases in the Au – Cd alloy system that is isoelectronic to the Cu-Zn alloy system [6]. The Au – Cd phase diagram is more complicated containing about 12 intermediate phases that are related to the basic high-symmetry structures as well as the structurally complex phases defined by Hume-Rothery rules. Formation of the larger number of the structures with many-faced BZ polyhedrons in the Au – Cd phases comparing to the Cu – Zn phases is stimulated by the higher atomic numbers and higher difference in atomic numbers of constituent elements.

In the present work we analyze necessary conditions for stability of the *fcc* structure and consider derivative complex structures. The subjects of analysis are the *sp* metals and binary alloys for which it is possible to assign a definite number of valence electrons.

2. Theoretical background and method of analysis

Formation of binary compounds at a certain alloy composition is defined by some important factors such as the difference in atomic sizes, electronegativity etc. Beyond these factors, formation of metallic structures is defined by effects of the Fermi sphere – Brillouin zone (FS-BZ) interaction. The Hume-Rothery mechanism has been identified to play a role in the stability of structurally complex alloy phases, quasicrystals and their approximants [7-11]. Jones model can be used to account for the phase stability in tetrahedral cluster structures, icosahedral and trigonal-prismatic clusters as building blocks. Formation of the complex structures of elemental metals under pressure can also be related to the Hume-Rothery mechanism [12-17].

The band structure contribution to the crystal structure energy can be estimated by analyzing configurations of Brillouin-Jones zone planes in the nearly free-electron model. A special program BRIZ has been developed [18] to construct FS-BZ configurations and to estimate some parameters such as the Fermi sphere radius (k_F), values of reciprocal wave vectors of BZ planes (q_{hkl}) and volumes of BZ and FS. The BZ planes are selected to match the condition $q_{hkl} \approx 2k_F$ that have a remarkable structure factor. In this case an energy gap is opened on the BZ plane leading to the lowering of the electron band energy. The ratio of $\frac{1}{2} q_{hkl}$ to k_F is usually less than 1 and equals ~0.95; it is called a "truncation" factor. In the FS-BZ presentations by the BRIZ program the BZ planes cross the FS, whereas in the real system the Fermi sphere is deformed and accommodated inside BZ. The "truncation" factor has a characteristic value and corresponds to a decrease in the electron energy on the BZ plane.

The crystal structure of a phase chosen for the analysis by the BRIZ program is characterized by the lattice parameters and the number of atoms in the unit cell, which define the average atomic volume (V_{at}). The valence electron concentration (z) is the average number of valence electrons per atom that gives the value of the Fermi sphere radius $k_F = (3\pi^2 z / V_{at})^{1/3}$. Further structure characterization parameters are the number of BZ planes that are in contact with the FS, the degree of "truncation" factor and the value of BZ filling by electronic states, defined as a ratio of the volumes of FS and BZ.

Presentations of the FS-BZ configurations are given with the orthogonal axes with the following directions in the common view: a* is looking forward, b* – to the right and c* – upward. For the hexagonal lattice in the reciprocal space $a^* = a_{1h}^* \cos 30^o$, $b^* = a_{2h}^*$ and $c^* = c_h^*$. Structural data for binary phases considered in this paper have been found in the Pauling File [19] and in recent papers cited in the corresponding sections of this paper.

3. Results and discussion

In this work we selected two groups of *fcc* based phases: elemental simple *sp* metals (Table 1) and binary alloy phases (Table 2). Diffraction patterns and constructed Brillouin-Jones zones for these structures are presented in Figures 1 and 2, respectively. Crystal structure description and element groups in the Periodic table are given following Pearson [20].

Table 1. Structure parameters of several metal phases with the fcc and fcc-based structures. Fermi sphere radius k_F, ratios of k_F to distances of Brillouin zone planes ½ q_{hkl} and the filling degree of Brillouin zones by electron states V_{FS}/V_{BZ} are calculated using the program BRIZ [18].

Phase	Cu(Zn)	α-Hg	β-Hg	Li	In	Te
Pearson symbol	*cF*4	*hR*1	*tI*2	*hR*3	*tI*2	*cF*4
			Structural data [a]			
Space group	$Fm\bar{3}m$	$R\bar{3}m$ *(h)*	*I*4/*mmm*	$R\bar{3}m$	*I*4/*mmm*	$Fm\bar{3}m$
T, P conditions		227K	77K	4.2K	Ambient conditions	255GPa
lattice parameters (Å)	$a = 3.698$	$a = 3.470$ $c = 6.719$ $c/a = 1.936$	$a = 3.995$ $c = 2.825$ $c/a = 0.707$	$a = 3.111$ $c = 22.86$	$a = 3.248$ $c = 4.946$ $c/a = 1.523$	$a = 3.757$
			FS – BZ data from the BRIZ program			
z (number of valence electrons per atom)	1.364	2	2	1	3	6
k_F (Å^{-1})	1.473	1.364	1.380	1.116	1.504	2.375
Total number BZ planes $k_F/(½\ q_{hkl})$	14	14	12	26	14	12
max	1.001	1.191	1.241	0.951	1.300	1.049
min	0.867	0.972	1.013	0.825	1.099	
V_{FS}/V_{BZ}	0.682	1.0	1.0	0.590	1.5	0.750

[a] Refs. [19-21]

3.1. Simple sp elements with the fcc-based structures

The *fcc* structure is one of the fundamental structures for metals along with *hcp* and *bcc* structures. These three atomic arrangements are characterized by high symmetry and close packing of atoms. It is interesting to consider chemical and physical factors that lead to the formation of complex and distorted phases – derivatives from these structures. Previously we have considered simple metal structures based on *bcc* and *hcp* [4,5] demonstrating the valence electron concentration as a defining factor of structural stability.

3.1.1. Fcc in the simple sp elements

The group I B elements Cu, Ag and Au crystallize in the *fcc* structure and do not change by variation of temperature or pressure, according to their name: "noble" metals. It should be noted that only for Au the *fcc* – *hcp* transition was found above 250 GPa [22].

The group I A elements Li and others adopt at ambient pressure the *bcc* structure and transform to *fcc* with the pressure increase [23]. The difference in the ambient pressure structure for univalent elements from I A and I B group can be explained by the balance of the electrostatic (Madelung) and the valence electron (band structure) terms in the crystal structure energy. Alkali I A elements adopt *bcc* predominantly under electrostatic energy because the Madelung constant is higher for *bcc*

Preprints (www.preprints.org) | NOT PEER-REVIEWED | Posted: 2 January 2017 doi:10.20944/preprints201701.0002.v1

Peer-reviewed version available at Crystals 2017, 7, 34; doi:10.3390/cryst7020034

structure than for *fcc* or *hcp*. Under pressure the band structure term increases leading to the formation of *fcc* for alkali metals.

The group I B elements follow the transition metals in the Periodic table and they have a filled *d*-electron band. Therefore there is some screening of E_{Ewald} and gaining of E_{BS}. The common view of the Fermi surface for Cu, Ag and Au is a sphere with necks extending to the Brillouin planes of the (111) type.

The *fcc* structure remains stable for elements I B in the sold solution with the neighboring elements II B and others. The limit of solubility is defined by the Hume-Rothery rule: at the valence electron concentration ~1.36 there is a contact of the Fermi sphere and the Brillouin Zone and the loss of stability for *fcc*. This case is shown for the Cu(Zn) alloy in Fig. 1a.

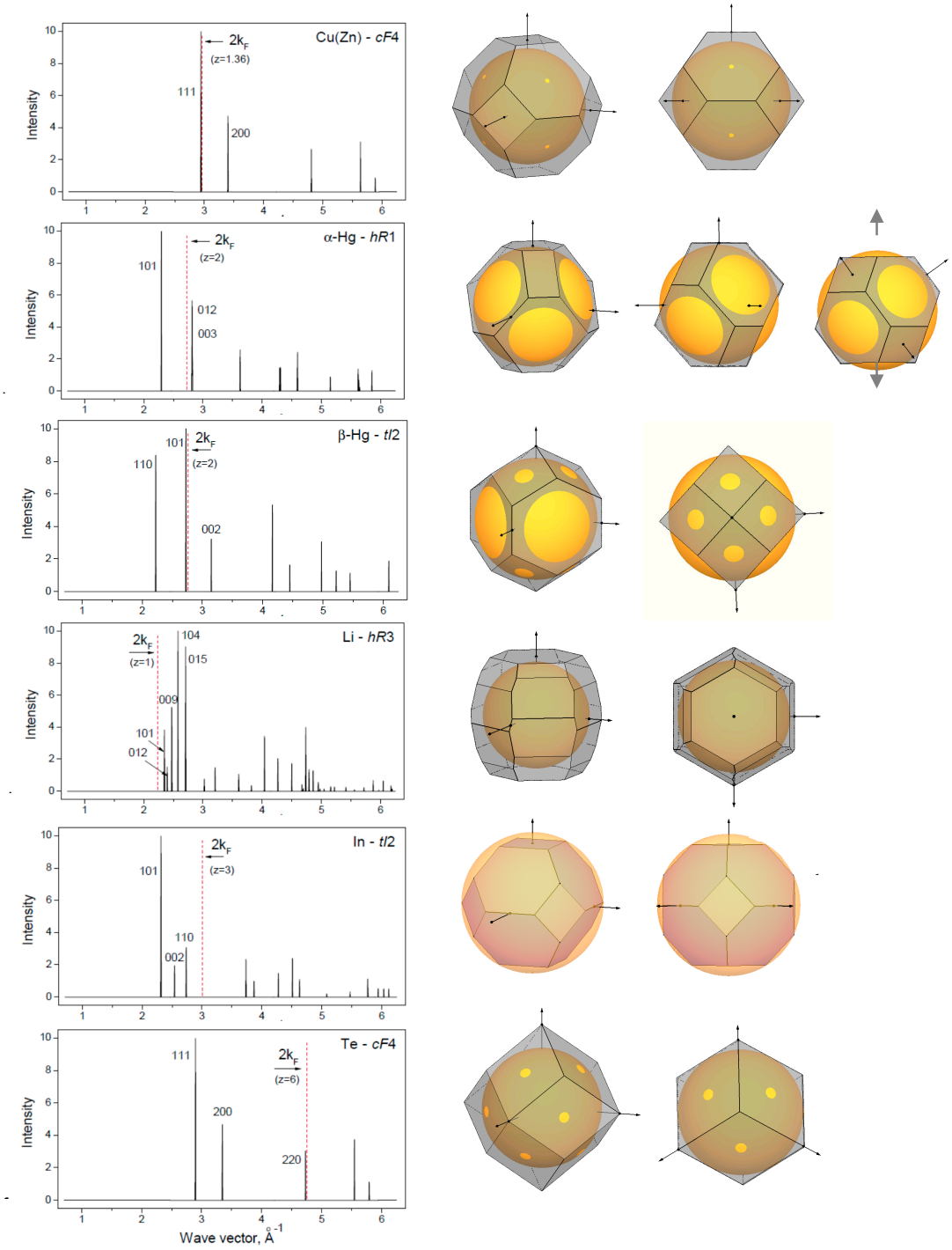

Figure 1. Calculated diffraction patterns for selected phases from Table 1 (left panel) and corresponding Brillouin-Jones zones with the Fermi spheres (right panel). The position of $2k_F$ and the

hkl indices of the planes used for the BZ construction are indicated on the diffraction patterns. Constructions of BZ-FS are given in common projection (first column) and in special projection (second column) (see text).

3.1.2. Distorted fcc structures of the II B element Hg

The light group II B elements Zn and Cd crystallize in the *hcp* structures with the elongated *c*/*a* ratio analyzed in [5]. The heavy II B element Hg adopts distortive *fcc* structures: *hR*1 for α-Hg an *tI*2 for β-Hg (Table 1). The rhombohedral α-Hg structure is closely related to *fcc*, as can be seen in Fig.1b from the construction of Brillouin zones for Hg-*hR*1 and for the hypothetical *fcc* with the same volume. BZ planes of the (111) type for *fcc* are divided into two sets of *hR*1 of (101) and (003) types in such way that the latter is placed outside FS at the same distance as (012) planes, which are the former (200)-*fcc* planes. Rhombohedral distortion degree is defined by the condition $\mathbf{q}_{003}=\mathbf{q}_{012}$ resulting in *c*/*a* = 1.936 for the rhombohedral cell in the hexagonal setting. This value is much lover than the ideal *c*/*a* = 2.45 for *fcc*. Hg-*hR*1 is obtained from *fcc* by contraction along one of the [111] axes as shown on Fig. 2b (right panel). Rhombohedral cell of *fcc* has 60° and Hg-*hR*1 structure has α = 70.52°. At low temperature and high pressure the β-Hg phase is stable.

The β-Hg structure can be described as a strong compression of *fcc* along c axis to *c*/*a* ~0.5. Standard description of β-Hg is as a body-centered tetragonal structure, *bct*, with *c*/*a* ~0.707 (close to $1/\sqrt{2}$). For this structure (101) planes are in contact with the FS as shown in Fig. 2c. Coordination number for Hg-*bct* is close to N=10.

The alloying of Hg with Sn under pressure was studied in [24]. The solubility of Sn in α-Hg was found to increase under pressure up to ~10 at.% Sn. The qualitative estimation for condition $k_F \sim \frac{1}{2}q_{012}$ gives the value z ~2.17 corresponding to ~8-9 at.% of a tetravalent metal and to ~17 at.% of a trivalent metal. The latter case is realized in the Hg-In system, where the α-Hg(In) solution extends to ~19 at.% In. Stability of the α-Hg(Sn) phase was observed to 30 GPa.

For pure Hg transformation α – β occurs under pressure ~3.4 GPa at room temperature with further transitions at 12 GPa to monoclinic structure (γ) and at 37 GPa to close-packed hexagonal structure [25,26]. Theoretical calculation [27] has shown that the *fcc* structure is extremely close to β- and γ-Hg. It should be noted that for II B elements Zn, Cd and Hg the common *hcp* phase exists under high pressure. The β-Hg phase is stabilized at ambient pressure in the Hg – Cd alloys at 4 to 70 at./% Cd [19]. This occurrence may be accounted for a chemical pressure because of atomic volume for Cd is less then for Hg (21.6 and 23.2 $Å^3$, respectively).

Preprints (www.preprints.org) | NOT PEER-REVIEWED | Posted: 2 January 2017 doi:10.20944/preprints201701.0002.v1

Peer-reviewed version available at Crystals 2017, 7, 34; doi:10.3390/cryst7020034

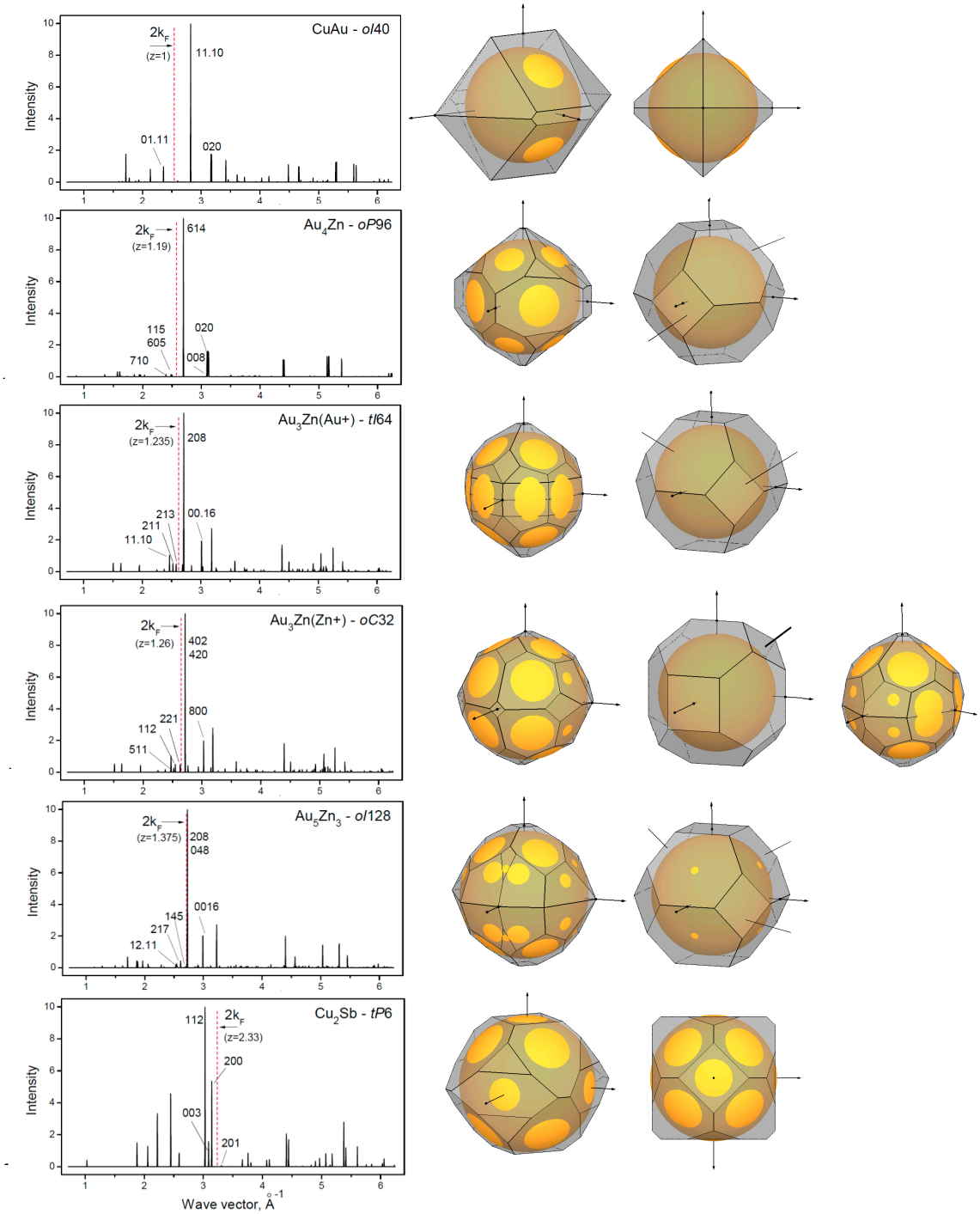

Figure 2. Calculated diffraction patterns for selected phases from Table 2 (left panel) and corresponding Brillouin-Jones zones with the inscribed Fermi spheres (right panel). The position of $2k_F$ and the hkl indices of the planes used for the BZ construction (first column) are indicated on the diffraction patterns. Constructions of BZ planes corresponding to the strong reflections (second column) show structural relationship to the basic cells (see text). For BZ of *o*C32 (d, third column) the projection is given along b* to show relation to *o*P128 (e).

3.1.3. Rhombohedral distortions of fcc in group I A element Li

Rhombohedral structure of α-Hg-*h*R1 type occurs in alkali element Li under pressure above 39 GPa after the transition *fcc*→*h*R1 [28]. Lattice parameter of Li-*h*R1 at 39.8 GPa are $a = 2.4023$ Å, $c = 5.516$ Å, $c/a = 2.296$ for the hexagonal cell and the rhombohedral angle is 62.87°. The degree of rhombohedral distortion of *fcc* is less than for α-Hg. With this deformation one set of the (111) planes

of BZ for *fcc* is placed closer to the FS corresponding to z=1, and there is some gain for the band structure energy term at the *fcc*→*hR*1 transition.

Another rhombohedral structure is known for Li and Na at low temperature at ambient pressure below 77 K and 25 K, respectively. This structure, usually defined as 9R or Sm-type, is close-packed structure with the sequence of hexagonal layers ABABCBCACA in contrast to the ABAB sequence for *hcp* and ABCABC for *fcc*. The physical source for energetic stability of the 9R phase was analyzed by Ashcroft using a Hume-Rothery argument [29]. The Brillouin-Jones zone of the 9R phase contains 26 planes that are close to the FS so that the overall electronic energy is reduced (see Table 1 and Fig.1d). The BZ for Li-*hR*3 is filled by electronic states upto 0.59 that is slightly more than 0.5 for Li-*bcc*.

3.1.4. Distortion of fcc in group III B elements

The lightest trivalent element Al has *fcc* structure and is found to be stable with the variation of temperature and pressure. This indicates to the importance of the electrostatic (Madelung) contribution into the crystal energy for this light element. Recently at very high pressure of 217 GPa the transformation *fcc* → *hcp* was observed for Al. For the heaviest III B metal thallium the valence electron contribution is significant and the resulting ambient pressure structure is *hcp*. Under pressure 3.7 GPa Tl transforms to *fcc* [30] and remains *fcc* up to 125 GPa [31].

The intermediate group III B metal In crystallizes at ambient pressure in a tetragonal structure that is a slight distortion of *fcc* with elongation of *c* axis to $c/a = 1.076$. Standard description of In structure is the body centered tetragonal, *bct* or *tI*2, as given in Table 1.

Physical reasons of the distorted In structure were considered within the model of Fermi sphere-Brillouin zone interactions [32]. The BZ polyhedron of *fcc* is deformed due to the attraction to the FS, in particular to the one set of corners of W' type. Dependence of *fcc* distortion is defined by the valence electron concentration and the ideal *fcc* is realized when the Fermi sphere contacts the BZ at the corners of W type: this case occurs for z = 2.94 electron/atom and is realized in the In alloys with Cd or Hg at about ~6 at.%. The structural distortion of *fcc* in In increases with the addition of 4-valent metals Sn or Pb up to 12-15 at.%. At higher electron concentration there is a phase transition to the *fct* with $c/a < 1$. The origin of existence of these two types of *fct* with $c/a > 1$ and $c/a < 1$ is related to different FS-BZ configurations where the FS is touched by the corners of BZ of W' or W type, as discussed in [13,32].

Similar tetragonal phase is formed in Ga – the lighter neighbor of In in III B group – under high pressure above 14 GPa with c/a ~1.12 (for *fct*). The Ga-*fct* phase has graduate transition to *fcc*, observed near 70 GPa [23,33]. Thus for group III elements the most abundant structure under compression is *fcc* or slightly distorted *fcc* structure.

3.1.5. High pressure fcc phase in polyvalent sp elements

The group VI B elements contain 6 *sp* electrons and their metallic phases obtained under pressure should be considered with respect not only to the first Brillouin zone but taking into account the planes of the larger Brillouin zones. An interesting case of the *fcc* structure was found recently for the group VI B element Te [34]. At normal pressure Te is non-metallic and its structure consists of a spiral chain (trigonal *hR*1) which transforms under pressure to some complex structures including an incommensurately modulated structure [23] with metallic properties. Above 27 GPa Te adopts the *bcc* structure, above 100 GPa it transforms to *fcc* with a superlattice and above 200 GPa to the *fcc* structure [34]. Consideration of Te-*fcc* phase with z = 6 shows the satisfaction to the FS-BZ interaction model (Table 1, Fig.1f). The FS contact with the BZ planes of the (220) type occurs for z = 5.92 and with z = 6 there is a slight overlap with the FS above $½q_{220}$, which is usual for the Hume-Rothery phases.

Iodine – the neighboring to Te element from group VII B – is a typical diatomic solid under ambient conditions. Transition to the metallic state has been found for Iodine above 16 GPa and several phases have been identified on the way from molecular to monatomic states including

incommensurate modulated structure [35]. At pressures above 55 GPa Iodine was found to crystallize in the *fcc* structure [36] which is stable to at least 273 GPa [37].

Appearance and stability of the *fcc* structure in the elements of groups VI B and VII B at high pressures is supported by the model of the FS-BZ interaction with consideration of the next Brillouin-Jones zones for polyvalent metals. In particular, for z = 6-7 the energetic gain is related to accommodation of the FS electrons into the BZ formed by (220) planes.

It should be noted that for group IV B elements the *fcc* appears the only for the heaviest element Pb at normal pressure and transforms under compression to *hcp* and then to *bcc*. For group V B elements the common high pressure phase is *bcc* (see reviews [13, 23]).

3.2. Binary alloy phases with the fcc based structures

For the binary alloys important factors of the phase formation are atomic size ratio and electronegativity. For our consideration we select group I B elements with the neighboring group elements with the minimal differences of these two factors that are however sufficient for site-ordered phase formation. In all cases it should be noted that the decisive factor for the structural stability is also the Hume-Rothery mechanism as is demonstrated for several representatives of binary phases (Table 2, Fig. 2).

Table 2. Structure parameters of several binary fcc-based phases from the literature data. Fermi sphere radius k_F, ratios of k_F to distances of Brillouin zone planes $\frac{1}{2} q_{hkl}$ and the filling degree of Brillouin zones by electron states V_{FS}/V_{BZ} are calculated using the program BRIZ [18].

Phase	CuAu	Au_4Zn	Au_3Zn (Au+)	Au_3Zn (Zn+)	Au_5Zn_3	Cu_2Sb
Pearson symbol	*oI*40	*oP*96	*tI*64	*oC*32	*oI*128	*tP*6
			Structural data [a]			
Space group T, P conditions	*Imma*	*Pnmn*	$I4_1/acd$	*Cmca* Ambient conditions	*Ibam*	*P*4/*nmm*
lattice parameters (Å)	*a* = 3.676 *b* = 3.956 *c* = 39.72	*a* = 24.216 *b* = 4.025 *c* = 16.244	*a* = 5.586 *c* = 33.40	*a* = 16.603 *b* = 5.581 *c* = 5.581	*a* = 5.510 *b* = 11.020 *c* = 33.620	*a* = 4.001 *c* = 6.104
			FS – BZ data from the BRIZ program			
z (number of valence electrons per atom)	1	1.19	1.235	1.26	1.375	2.33
k_F (Å^{-1})	1.27	1.288	1.310	1.322	1.367	1.618
Total number BZ planes	14	28	50	34	34	22
$k_F/(\frac{1}{2} q_{hkl})$						

Preprints (www.preprints.org) | NOT PEER-REVIEWED | Posted: 2 January 2017 doi:10.20944/preprints201701.0002.v1

Peer-reviewed version available at Crystals 2017, 7, 34; doi:10.3390/cryst7020034

max	1.0078	1.0756	1.0635	1.069	1.046	1.0686
min	0.7996	0.825	0.8705	0.873	0.914	0.979
V_{FS}/V_{BZ}	0.600	0.875	0.972	0.968	0.921	0.916

[a] Refs. [19-21]

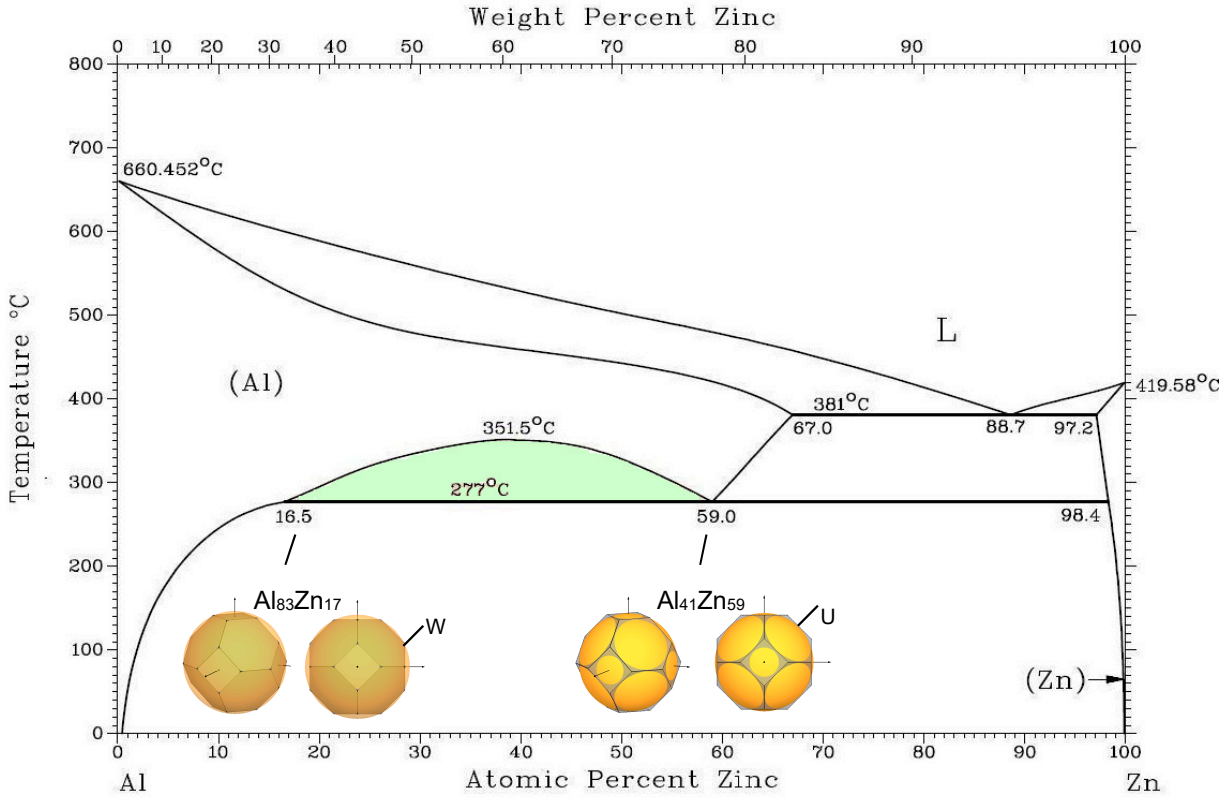

Figure 3. The phase diagram Al – Zn [*19*]. The Al(Zn) solid solution region with the *fcc* structure contains a miscibility gap with two-phase region (colored). For the boundary phases with 17 and 59 at% Zn constructions of FS-BZ are given with a common view and a view along a* (see text).

3.2.1. Long-period superlattice in the CuAu alloy

Cu and Au are both univalent group I B metals with the atomic size difference ~12%. The CuAu alloy forms the tetragonally distorted *fcc* lattice where alternate (00h) planes contain either Cu or Au atoms and cause a contraction in *c* direction. Resulting tetragonal face-centered structure has *c*/*a* ratio of 0.92 [19]. In the temperature range ~380°C to 410°C the superlattice CuAu II is formed which consist of CuAu-*bct* unit cells with the antiphase domains along the *b* direction. There is a lattice shift of ½(*a*+*c*) at each five unit-cell length [38,39]. The superlattice CuAuII is described as orthorhombic cell with 10 cells along one of a direction, *oI*40.

The stabilization of long-period superlattices in CuAu and other alloys has been understood by considering that the Fermi surface touches the newly formed superlattice Brillouin zone boundaries {110} that are adjusted due to the formation of an extra period. Fig. 2a is showing the touching of the Fermi sphere to the planes (01.11). The degree of overlapping (½ q_{hkl}) / k_F for ideal FS is usually ~0.95 as was considered by Sato and Toth [38] and is called a "truncation" factor. In our paper we use the reciprocal value to characterize the FS-BZ interaction in all considered cases.

3.2.2. Binary alloy Au – Zn phases based on the fcc structure

The Cu(Zn) *fcc* solid solution (considered above in the section *3.1.1.*) exists up to the electron concentration z = 1.36 without any ordered phases at low temperatures. For alloys with Au(Zn), the

fcc structure exists at high temperature (403 – 683°C) within the same region of the electron concentration (upto 33% Zn). However a number of ordered phases with long-period superlattices were found at low temperature [19]. Single crystal studies of 19, 23.5 and 26 at.% Zn by X-ray diffraction [40,41] allow structure characterization of these phases. We consider possible mechanism of structural stability due to formation of additional Brillouin zone plane causing lattice modulations (Table 2, Fig. 2b-e).

For the Au_4Zn-*oP*96 structure, the superlattice cell is related to the basic *fcc* cell (with a_f parameter) with a model: $a = 6a_f$, $b = a_f$ and $c = 4a_f$ [32]. Atomic positions are varied corresponding to the lattice modulation. In Fig.2b the new BZ boundaries of the (115) and (710) types are shown crossing the FS whereas for the basic BZ (shown right) there is no contact with FS. The phase stabilization is considered to be due to the formation of the new BZ planes in contact with the FS which is reducing the crystal energy.

$Au_{3+}Zn$-*tI*64 phase is related to *fcc* in the following way: $a = \sqrt{2}a_f$, $c = 8a_f$. Atomic shifts produce extra diffraction reflections [42] resulting in the BZ boundaries enveloping the FS (Fig. 2c).

Au_3Zu_{+}-*oC*34 phase occurs through a phase transition from *fcc* in a similar way with b and $c \sim \sqrt{2}a_f$ and $a = 4a_f$ (standardized data are used). FS-BZ construction is given in Fig. 2d showing relation of two Au_3Zn phases with slight difference in composition.

Au_5Zn_3-*oI*128 phase has also a relation to *fcc* and occurs at the alloy concentration boundary for the *fcc* stability. Cell parameters are produced from *fcc* cell in the following way: $a = \sqrt{2}a_f$, $b = 2\sqrt{2}a_f$ and $c = 8a_f$, resulting in 32 *fcc* cells with 128 atoms (Fig.2e). Thus in the Au – Zn alloy system in the composition range up to ~40 at.% Zn, there are several complex phases that are superlattices based on *fcc*. Formation of these superstructures is related to the Hume-Rothery mechanism.

3.2.3. Defect structures based on fcc

In this section we consider another way of the structure adjustment to the Hume-Rothery rules via formation of defect structures with vacancies. For γ-brass in Cu – Ga and β-(NiAl) it was found that with increasing the average number of valence electrons z these structures can be stabilized by skipping atoms out of the unit cell. Thus, for stability of the phase it is fundamental to keep the constant number of electrons per unit cell zN. In the Cu – Ga alloy systems, the γ-brass exists in the wide range of compositions 30-43 at.% Ga and the number of atoms in the unit cell was found to decrease from 52 to 47 atoms [43].

A special case of defect superstructure is vacancies at certain atomic positions in the cell. The structure Cu_2Sb-*tP*6 is related to the tetragonal distortion of the *fcc* with the double cell along *c* axis and with the absence of Cu atoms in the middle of *c*. Resulting number of atoms in the cell is N = 6 and the constructed FS-BZ configuration satisfies he Hume-Rothery mechanism (Fig.2f). Similar *tI*6 structure is found in Cu_2As.

It is remarkable that Cu_2Sb-*tP*6 type structure is formed in the Cu-Te alloy at the composition of 41.7 at.% Te [19]. Because Te is an element from the next group (VI B) after the group of Sb (V B) there are more vacancies of Cu atoms for basic Cu positions 2c and 2a with occupation 0.7 which gives the resulting number of atoms N = 4.8 in the unit cell instead of N = 6 for Cu_2Sb. This is the response of the crystal structure to FS-BZ interactions for the phase $Cu_{1.4}Te$.

Another example of defect supercell formation based on *bcc* is $CuGa_2$-*tP*3 with two *bcc* cells along c axis and with missing Cu atoms in the middle of *c*. There is the way to adjust structure to the number of valence electrons in the cell.

3.3. Miscibility gap of two fcc phases in the Al – Zn alloys

For polyvalent metals the volume of the valence electrons, defined by the volume of the Fermi sphere, is always large than the volume of the BZ. Therefore the Fermi surface cuts many zone planes and contributions to the crystal energy from regions near the plane intersections may lead to important effects for phase stability [44].

An interesting case of the *fcc* phase decomposition is observed in the Al – Zn alloy system, where Al(Zn) *fcc* solid solution is stable at high temperature and below 352°C there is a miscibility gap of

two *fcc* phases with 16.5 and 59 at.% Zn. The atomic radii of Al and Zn are very close (1.43 Å and 1.37 Å, respectively) and electronegativities are nearly equal (1.61 and 1.65), so there must be some other factor that defines the decomposition [20]. In this case it is the electronic structure factor(See Figure 3). Theoretical consideration of the electronic topology in the *fcc* Al – Zn alloys has been performed in Ref. [45].

We consider coexistence of two *fcc* Al(Zn) phases with the configuration of FS and BZ. It was discussed for In-*fcc* phase that the important factor for the structure stability is BZ accommodation within the Fermi sphere. The contact of FS with W-type corners occurs for z = 2.94 which corresponds to addition of ~7% Zn and due to the "truncation" factor can be extended to z = 2.83 which corresponds to ~17at.%Zn as observed in one of the *fcc* Al-Zn phase. Another factor for gaining in energy for *fcc* is a contact to the edges of (111) planes in the points K and U of BZ that occurs at z = 2.5 for ~50 at.% Zn. This results in the "truncation" factor 1.036 – very acceptable for the Hume-Rothery conditions. It should be noted that the region of miscibility gap of the two Al(Zn) *fcc* extends under pressure along the temperature [46] in accordance to the common trend that an energy gap increases under pressure.

4. Conclusion

The phase sequence in the Cu – Zn alloy system consists of simple high-symmetry metallic structures *fcc*, *bcc* and *hcp* (α, β and ε) with an addition of two phases (γ-*cI*52 and δ-*hP*3) that are derivatives of the *bcc* structure. Phases α, β and ε are completely site-disordered because Cu and Zn, the constituent elements of the alloy, are close neighbors in the periodic table and have minimal differences in the atomic size and electronegativity. In the Au – Zn alloy system in the composition range up to ~40 at.% Zn, there are several complex phases that are superlattices based on *fcc*. Formation of these superstructures is related to the Hume-Rothery mechanism. Additional complexity of the Au – Zn alloys in comparison to the Cu – Zn alloys is related to the larger difference in atomic numbers of the alloy components that provides relatively strong diffraction peaks for site-ordered compounds. Remarkable example is a long-period superlattice of the CuAu with the size of domains defined by formation of superstructure reflections in contact to the Fermi sphere [38].

In the pure simple *sp* elements the *fcc* phase is stable in group I B metals (Cu, Ag, Au) and their solid solutions up to ~1.35 electron/atom. In this case the FS is inside the first BZ and touched the (111) planes. For the group III B element In the *fcc* structure shows a tetragonal distortion which can be understood through the BZ deformation: FS accommodates the BZ by touching one type of the W corners. Similar tetragonal face-centered structure is observed for compressed Ga. The contact of the FS with the special points of BZ such as W-type corners or the edges of (111) planes of BZ in the points K and U can lead to a miscibility gap between two *fcc* phases as in the case of Al – Zn alloys.

In conclusion of this discussion it should be noted that the *fcc* phase appears under pressure for group I A (alkali metals) and is followed by complex structures that show a decrease in coordination number and packing density (for Li and Na after *cI*16, for Rb and Cs after *oC*52 and *oC*84, respectively) [13,23]. The reason of unexpected structural complexity for alkalis under strong compression can be understood if one accepts the change in the valence electron number due to the overlap of the valence band and upper core electron levels [14,15]. Thus, the application of the FS-BZ interaction model allows us to estimate the effective number of valence electrons in the case of the change of the valence electron state and also for complex *spd* valence states.

Acknowledgments: The authors gratefully acknowledge Dr. Olga Degtyareva for valuable discussion and comments. This work is supported by the Program "The Matter under High Pressure" of the Russian Academy of Sciences.

References

[1] W. Hume-Rothery, Researches on the nature, properties, and condition of formation of intermetallic compounds, J. Inst. Metals. 35, (1926) 319-335.

[2] N.F. Mott, H. Jones, The Theory of the Properties of Metals and Alloys, Oxford University Press, London, 1936.

[3] H. Jones, The Theory of Brillouin Zones and Electron States in Crystals, North Holland, Amsterdam, 1962.

[4] V.F. Degtyareva, N.S. Afonikova, Simple metal binary phases based on the body centered cubic structure: Electronic origin of distortions and superlattices, J. Phys. Chem. Solids 74 (2013) 18-24.

[5] V.F. Degtyareva, N.S. Afonikova, Simple metal and binary alloy phases based on the hcp structure: Electronic origin of distortions and superlattices, Solid State Sciences 37 (2014) 47-54.

[6] V.F. Degtyareva, N.S. Afonikova, Complex structures in the Au-Cd alloy system: Hume-Rothery mechanism as origin, Solid State Sciences 49 (2015) 61-67.

[7] S. Lee, R. Henderson, C. Kaminsky et al., Pseudo-fivefold diffraction symmetries in tetrahedral packing, Chem. Eur. J. 19 (2013) 10244–10270.

[8] U. Mizutani, Hume-Rothery Rules for Structurally Complex Alloy Phases, Taylor & Francis, London, 2010.

[9] R.F. Berger, P.L. Walters, S. Lee, R. Hoffmann, Connecting the chemical and physical viewpoints of what determines structure: from 1-D chains to gamma-brasses, Chem. Rev. 111 (2011) 4522–4545.

[10] S. Lee, C. Leighton, F.S. Bates, Sphericity and symmetry breaking in the formation of Frank–Kasper phases from one component materials, Proc. Natl. Acad. Sci. USA 111 (2014) 17723-17731.

[11] J. Feng, R. Hoffmann, N.W. Ashcroft, Double-diamond NaAl via pressure: Understanding structure through Jones zone activation, J. Chem. Phys. 132 (2010) 114106.

[12] V.F. Degtyareva, Brillouin zone concept and crystal structures of sp metals under high pressure, High Press Res. 23 (2003) 253-257.

[13] V.F. Degtyareva, Simple metals at high pressures: The Fermi sphere - Brillouin zone interaction model, Physics-Uspekhi. 49 (2006) 369-388.

[14] V.F. Degtyareva, O. Degtyareva, Structure stability in the simple element sodium under pressure, New J. Phys. 11 (2009) 063037.

[15] V.F. Degtyareva, Potassium under pressure: Electronic origin of complex structures, Solid State Sciences 36 (2014) 62-72.

[16] V.F. Degtyareva, Structural simplicity and complexity of compressed calcium: electronic origin, Acta Crystallogr. B 70 (2014) 423-428.

[17] V.F. Degtyareva, Electronic Origin of the Orthorhombic Cmca Structure in Compressed Elements and Binary Alloys, Crystals 3 (2013) 419-430.

[18] V.F. Degtyareva, I.S. Smirnova, BRIZ: a visualization program for Brillouin zone – Fermi sphere configuration, Z. Kristallogr. 222 (2007) 718-721.

[19] P. Villars, K. Cenzual (Eds.), Pauling File Binaries Edition, ASM International, Metal Park, OH, 2002.

[20] W.B. Pearson, The Crystal Chemistry and Physics of Metals and Alloys, Wiley, New York, 1972.

[21] W.B. Pearson, A Handbook of Lattice Spacings and Structures of Metals, Vol. 2, New York, Pergamon Press, 1967.

[22] L. Dubrovinsky, N. Dubrovinskaia, W.A. Crichton, A.S. Mikhaylushkin, S.I. Simak, I.A. Abrikosov, J.S. de Almeida, R. Ahuja, W. Luo, and B. Johansson, Phys. Rev. Lett. 98 (2007) 045503.

[23] M.I. McMahon, R.J. Nelmes, High-pressure structures and phase transformations in elemental metals, Chem. Soc. Rev. 35 (2006) 943–963.

[24] V.F. Degtyareva, I.K. Bdikin, F. Porsch, N.I. Novokhatskaya, The stability of the rhombohedral α-Hg phase alloyed with Sn under high pressure up to 30 GPa, J. of Phys. Condens. Matter 15(2003) 7489-7500.

[25] K. Takemura, H. Fujihisa, Y. Nakamoto, S. Nakano and Y. Ohishi, Crystal Structure of the High-Pressure Phase of Mercury: A Novel Monoclinic Distortion of the Close-Packed Structure, J. Phys. Soc. Japan 76 (2007) 023601.

[26] K. Takemura, S. Nakano, Y. Ohishi, Y. Nakamoto and H. Fujihisa, High-pressure structural study of solid mercury up to 200GPa, Mater. Res. Express 2 (2015) 016502.

[27] S. Biering, P. Schwerdtfeger, High-pressure transitions in bulk mercury: a density functional study, Theor. Chem. Acc. 130 (2011) 455–462.

[28] M. Hanfland, K. Syassen, N.E. Christensen and D.L. Novikov, New high-pressure phases of lithium, Nature 408 (2000) 174–178.

[29] N.W. Ashcroft, Quantum-solid behavior and the electronic structure of the light alkali metals, Phys. Rev. B 39 (1989) 10552-10559.

[30] O. Schulte, A. Nikolaenko and W.B. Holzapfel, Pressure-Volume Relations For Zn, Cd, Ga, In And Tl At Room Temperature To 30 GPa And Above, High Press. Res. 6 (1991) 169-182.

[31] C. Cazorla, S.G. MacLeod, D. Errandonea, K.A. Munro, M.I. McMahon and C. Popescu, Thallium under extreme compression, J. Phys.: Condens. Matter 28 (2016) 445401.

[32] O. Degtyareva, V.F. Degtyareva, F. Porsch, and W.B. Holzapfel, Face-centred cubic to tetragonal transitions in In alloys under high pressure, J. of Physics: Condensed Matter 13 (2001) 7295-7303.

[33] O. Degtyareva, M.I. McMahon, D.R. Allan and R.J. Nelmes, Structural Complexity in Gallium under High Pressure: Relation to Alkali Elements, Phys. Rev. Lett. 93 (2004) 205502.

[34] T. Sugimoto, Y. Akahama, T. Ichikawa, H. Fujihisa, N. Hirao, Y. Ohishi, Bcc-fcc structure transition of Te, J. of Physics: Conference Series 500 (2014) 192018.

[35] K. Takemura, K. Sato, H. Fujihisa, M. Onoda, Modulated structure of solid iodine during its molecular dissociation under high pressure, Nature 423 (2003) 971-974.

[36] Y. Fujii, K. Hase, N. Hamaya, Y. Ohishi, A. Onodera, O. Shimomura, and K. Takemura, Pressure-induced face-centered-cubic phase of monatomic metallic iodine, Phys. Rev. Lett. 58, (1987) 796-799.

[37] R. Reichlin, A. McMahan, M. Ross, S. Martin, J. Hu, R. Hemley, H. Mao, Y. Wu, Optical, X-ray, and band-structure studies of iodine at pressures of several megabars, Phys. Rev. B 49 (1994) 3725-3731.

[38] H. Sato, R.S. Toth, Fermi surface of Alloys, Phys. Rev. Lett. 8 (1962) 239-241.

[39] H. Sato, R.S. Toth, Long-Period Superlattices in Alloys. II, Phys. Rev. 127 (1962) 469-484.

[40] H. Iwasaki, M. Hirabayashi, K. Fujiwara, D. Watanabe, S. Ogawa, Study on the Ordered Phases with Long Period in the Gold-Zinc Alloy System I. Survey of Crystal Structures and Calorimetric Measurement, J. Phys. Soc. Jpn. 15 (1960) 1771-1783.

[41] O. Terasaki, Study of the Incommensurate Two-Dimensional Antiphase Structure of $Au_{3+}Zn$ by High Voltage, High Resolution Electron Microscopy, J. Phys. Soc. Jpn. 51, (1982) 2159-2167.

[42] H. Iwasaki, Study on the Ordered Phases with Long Period in the Gold-Zinc Alloy System II. Structure Analysis of $Au_3Zn[R_1]$, $Au_3Zn[R_2]$ and $Au_{3+}Zn$, J. Phys. Soc. Jpn. 17 (1962) 1620-1633.

[43] J.O. Betterton, W. Hume Rothery, The Equilibrium diagram of the system copper - gallium in the region 30-100 at.% gallium, Journal of the Institute of Metals 80 (1952) 459-468.

[44] V. Heine, D. Weaire, Pseudopotential Theory of Cohesion and Structure, in: H. Ehrenreich, F. Seitz, D. Turnbull (Eds.) Solid State Phys. Academic, New York, 1970, 24, pp. 249-463.

[45] E.A. Smirnova, P.A. Korzhavyi, Yu.Kh. Vekilov, B. Johansson, I.A. Abrikosov, Electronic topological transitions and phase stability in the fcc Al-Zn alloys, Eur. Phys. J. B 30 (2002) 57–66.

[46] Y. Fujinaga, S. Tasaku, The aluminum-zinc phase diagram under high pressure, J. of Alloys and Compounds 209 (1994) 311-317.